External noise imposed on the reaction-diffusion system $CO+O_2 \rightarrow CO_2$ on Ir(111) surfaces: Experiment and theory

Yumino Hayase,[1,2,*] Stefan Wehner,[3] Jürgen Küppers,[3,4] and Helmut R. Brand[1]
[1]*Theoretische Physik III, Universität Bayreuth, 95440 Bayreuth, Germany*
[2]*Department of Physics, Kyushu University, Fukuoka 812-8581, Japan*
[3]*Experimentalphysik III, Universität Bayreuth, 95440 Bayreuth, Germany*
[4]*Max-Planck-Institut für Plasmaphysik, 85748 Garching, Germany*
(Received 3 September 2003; published 27 February 2004)

We study experimentally and theoretically the influence of noise on the fractions of CO and oxygen in the constant gas flow directed at an Ir(111) surface during CO oxidation. Depending on the noise strength and the fraction Y of CO we observe in the deterministically bistable region a large variety of different types of behavior. These include bistable behavior for small noise intensities, transitions from the upper to the lower branch of the bistable loop and vice versa, island nucleation and growth and noise-induced switching. Near the boundary of the bistable region and in the presence of noise the transition between the two branches takes place via very slow domain wall motion with time scales of the order of 10^4–10^5 s. The experiments were carried out in an UHV system for which the mass flow could be controlled very precisely. The modeling was using the reaction-diffusion system underlying the reaction studied for which all the kinetic coefficients are known rather precisely. Our numerical analysis was performed for one and two spatial dimensions showing qualitatively similar behavior. The comparison between the experimental results and the modeling shows semiquantitative to quantitative agreement.

DOI: 10.1103/PhysRevE.69.021609 PACS number(s): 82.40.Ck, 82.40.Np, 05.40.−a

I. INTRODUCTION

A. Theory

The study of the influence of noise on macroscopic systems is a classical field of physics [1]. We mention as an example the evaluation of the escape rate of a system over a barrier (Kramers' problem [2]). Frequently the noise encountered is additive, that means in a equation describing the time evolution of a system for one or more ''stochastic'' variables one has as driving force a deterministic part and a noise force, which does not depend on the variable. When certain conditions for the deterministic forces (detailed balance) are satisfied [3–5], one can derive a generalized thermodynamic potential for the case of Gaussian white noise.

If a given dynamical system has only one stable fixed point and the noise is additive, the stationary probability distribution has its maximum at this point (for the type of systems discussed). The situation becomes more complex if one has not only one, but say two stable and one unstable fixed points. In case there exists a generalized thermodynamic potential associated with such a system, the stationary probability distribution will have two humps and a minimum in between. A typical example for such a behavior is the absorptive optical bistability in nonlinear optics [6,7]. Except for one parameter value, the two minima of the associated generalized thermodynamic potential are not equal in depth (the peaks in the stationary probability distribution are not equally high). This implies that one of the minima is a global minimum whereas the other one is a local minimum. As a function of a parameter, for example, the external laser field in the case of optical bistability, one traces a sigmoidal shaped curve in parameter space consisting of two stable (at least locally) branches (upper and lower branch) and one unstable branch in between (compare also Fig. 1 below for the analogous plot in the present system).

A very similar picture emerges frequently when a potential is not known. In this case one has then, for example, two different attractors: one that has a larger basin of attraction (corresponding to the deeper well in the potential case), while the other deterministically stable fixed point has a smaller basin of attraction and corresponds to a well which is more shallow in the potential picture. For the system studied in this paper, the oxidation of CO on Ir(111) during admission of a constant CO + oxygen flux to the surface, we have sketched out this situation in Fig. 2. The oxygen surface areal density is plotted as a function of the CO surface areal density. A variation of the CO fraction Y in the flux leads to a change from a big basin of attraction for the upper branch, that is, the O rich surface [Fig. 2(a)] to a smaller basin of attraction for the upper branch [Fig. 2(b)]. Even in the nonpotential case one uses frequently the terms deeper and shallower well as a shorthand notation, and we will follow this custom.

Bistable systems occur in many branches of physics, not only in optics. Another example where such systems are discussed frequently, in particular in recent years, are chemical reactions (compare, for example, Refs. [8–12], and references therein). And, indeed, the subject of our combined experimental and theoretical studies described in the following is a chemical reaction on a surface.

So far we have only talked about additive noise. But it is also possible to have a noise source, which depends on the stochastic variable(s) characterizing the system. It could, for example, multiply the variable x with the noise strength ξ:

*Email address: yumino@stat.phys.kyushu-u.ac.jp

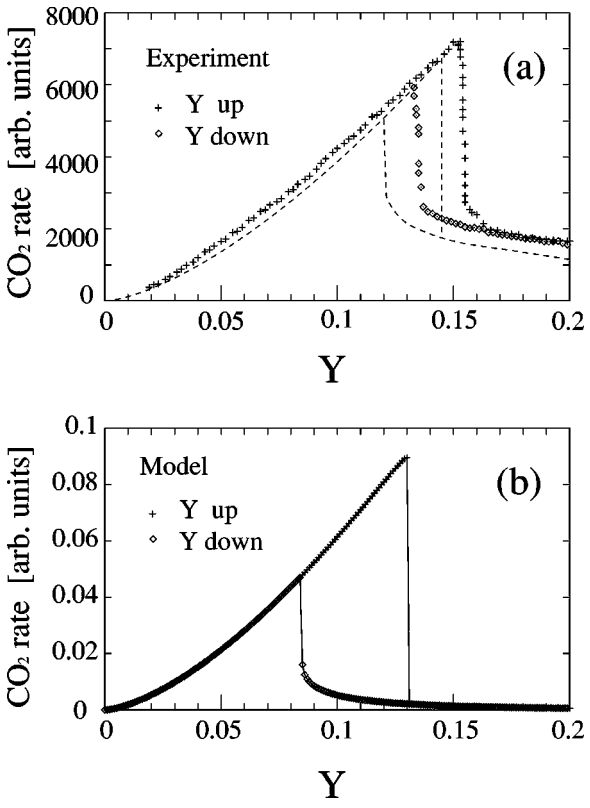

FIG. 1. (a) CO_2 rate measured during admitting CO and oxygen to Ir(111) surfaces at $T=500$ K and constant total flux $\Phi=0.88$ ML/s. Y denotes the CO fraction in this flux. The dashed lines indicate the position of the hysteresis reported in Ref. [24]. See the text for details. (b) This plot shows the deterministic hysteresis loop for the CO_2 rate as a function of $Y=\Phi_{CO}/\Phi_{total}$ for $T=500$ K as resulting from the kinetic model equations. The parameter values used for the kinetic coefficients are $\Phi=1.37\times10^{15}$ cm^{-2} s^{-1}, $n_{Ir}=1.56\times10^{15}$ cm^{-2}, $s_{CO}=1$, $\nu_{CO}=1\times10^{13}$ s^{-1}, $E_{CO}=140$ kJ/mol, $\nu_{rea}=10^5$ ML^{-1} s^{-1}, $E_{rea}=40$ kJ/mol, and $s_O=0.11$ and $x=3$. The bistable regime extends from $Y=0.084$ to $Y=0.131$. The speed of domain walls passes through 0 close to $Y=0.109$. In both plots the ordinate is in arbitrary units (arb. units).

$x\xi$. In this case the term multiplicative noise is used [13]. This type of noise can have dramatic and often qualitative consequences for the resulting probability distributions: their maxima can be shifted away from the locations of the deterministically stable states and the number of maxima of the stationary probability distribution can change as a function of the noise strength [14]. As for the time dependence, one can encounter a change from purely exponential relaxation to nonexponential behavior [13]. Experimentally the influence of multiplicative noise has been studied for electronic systems [15] without spatial degrees of freedom as well as for systems for which spatial degrees of freedom are important, for example, for electroconvection in nematic liquid crystals [16].

If the noise contributes in an additive as well as in a multiplicative manner, as is the case studied in the following, a combination of the phenomena outlined above will typically occur.

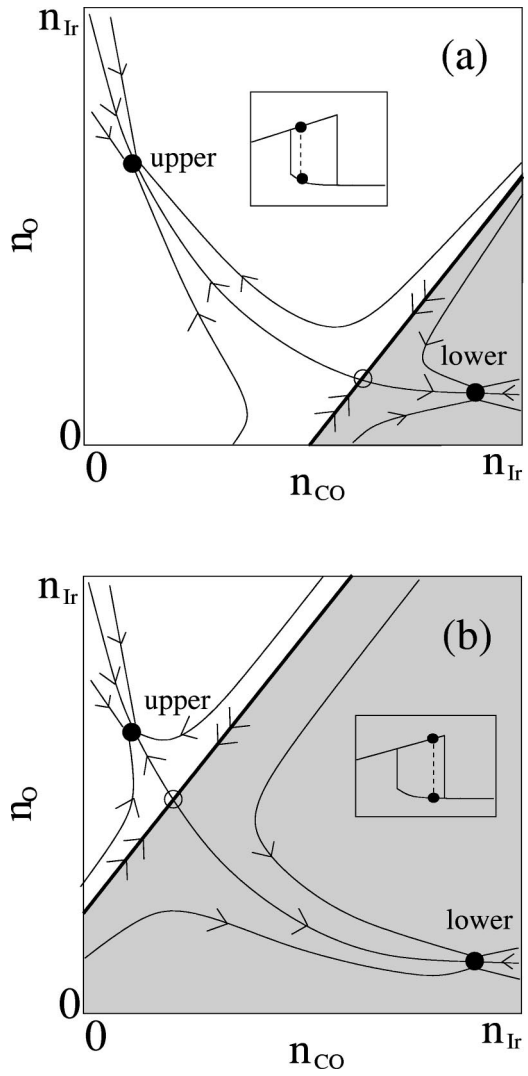

FIG. 2. The oxygen surface areal density, n_O, is plotted as a function of the CO surface areal density, n_{CO}. Both areal densities are bounded by the availability of Ir sites, n_{Ir}. The thin solid lines are examples of trajectories on the n_O-n_{CO} plane, which illustrate how the system will move from arbitrary initial conditions (n_O^0, n_{CO}^0) towards the stable fixed points. A variation of the CO fraction Y in the flux leads to a change from a big basin of attraction for the upper branch [Fig. 2(a) on top] to a smaller basin of attraction for the upper branch [Fig. 2(b)]. Note that the separatrix (thick black solid line) delineates the borderline between the basins of attraction for the upper branch (white) and that of the lower branch (gray), where the Y value in (a) is smaller than the Y value in (b).

In the theoretical description given so far, we have not mentioned the influence of spatial degrees of freedom (that is, we have looked at the zero-dimensional case). However, the system studied, the CO oxidation reaction on Ir(111) surfaces, has clearly spatial extent. As a consequence we must incorporate into our investigations both the noise forces as well as the spatial degrees of freedom and we also take into account the interactions between these two types of contributions. The latter type of effects leads, for example, to a natural explanation of the very long transients observed experimentally for the surface reaction studied in terms of

nucleation and wall motion in one and two spatial dimensions mediating the transition from the upper to the lower branch and vice versa. We also emphasize that the combination of externally controllable multiplicative and additive noise studied here is rather unique. In fact, we are not aware of any previous experiment for which a well-defined combination of additive and multiplicative noise has been applied externally.

B. Experiment

The CO oxidation reaction on a well-characterized single crystal surface can provide an exceptionally well-defined example of a bistable reaction-diffusion system. On surfaces of the Pt group metals, which neither strongly oxidize nor dissociate CO upon its adsorption, formation of CO_2 is readily observed. If the surface exhibits structural instability with respect to adsorption of one of the reactants, the CO_2 reaction rate at fixed CO and oxygen fluxes directed at the surface exhibits oscillatory behavior [17–19]. If it is structurally stable, the reaction rate might display bistability, i.e., the CO_2 rate exhibits a hysteresis in the rate/reactants composition diagram. Accordingly, at a total gas flux Φ of CO and oxygen and given CO fraction Y in this flux there are two possible CO_2 rates, high or low, which might be achieved either by increasing Y from 0 upwards or decreasing Y from 1 downwards.

Structurally stable and sufficiently reactive with respect to CO oxidation are (111) surfaces of Pd, Pt, and Ir. As an example, the CO_2 reaction kinetics on Pt(111) has been shown to exhibit bistability upon changing the CO/oxygen ratio in a simultaneously varied total gas flux impinging the catalyst surface [20–22]. A reaction kinetics hysteresis was also observed in a more complicated reaction, NO reduction with hydrogen on Rh and Ir surfaces [23].

Very recently it was shown by coauthors of the present work that the kinetics of the CO oxidation reaction on Ir(111) surfaces exhibits bistability [24]. Unlike previous studies, these and the present experiments were performed according to the rules implied in theoretical descriptions of the respective reactions, i.e., Φ constant, Y varied. The experiments employed very long ($>10h$) measuring times for approach to the CO_2 equilibrium rates in order to warrant that the influence of transient effects could be neglected. The CO_2 rates obtained at 500 K, a total CO + oxygen flux of 0.88 ML/s (1 ML$=1.56\times10^{15}$ cm^{-2}, the areal density of atoms on the Ir(111) surface), and varied Y fraction of CO in this flux are shown in Fig. 1.

It is seen that in the range $0.135<Y<0.155$ the CO_2 rates exhibit bistability with a high rate and a low rate branch, the former obtained upon ramping Y up, the latter upon ramping Y down. At a fixed Y value within the hysteresis limits, through application of short pure CO gas pulses the CO_2 rate could be switched from the high rate branch to the low rate branch, and vice versa using oxygen pulses.

In order to rationalize this phenomenon, the appropriate set of reaction kinetics differential equations (RKDEs) was set up and for the zero-dimensional approach, i.e., neglecting diffusion on a spatially extended surface, one gets

$$dn_{CO}/dt = s_{CO}\Phi Y n_e/n_{Ir} - \nu_{CO} n_{CO} \exp(-E_{CO}/kT) - \nu_{rea} n_{CO} n_O \exp(-E_{rea}/kT), \quad (1)$$

$$dn_O/dt = 2 s_O \Phi (1-Y)(n_e/n_{Ir})^x - \nu_{rea} n_{CO} n_O \exp(-E_{rea}/kT) \quad (2)$$

$$dn_{CO_2}/dt = \nu_{rea} n_{CO} n_O \exp(-E_{rea}/kT), \quad (3)$$

with s_{CO}, s_O as CO and oxygen sticking coefficients, respectively, $s_{CO}=1$ set for simplicity; Φ as combined gas flux of CO and oxygen; Y as fraction of CO in this flux; n_{Ir}, n_e, n_{CO}, and n_O as surface areal densities of Ir atoms, empty, CO, and O occupied sites, respectively; the normalizing condition $n_{CO}+n_O+n_e=n_{Ir}$ applies; ν_{CO} and E_{CO} as desorption frequency factor and desorption activation energy of CO; ν_{rea} and E_{rea} as reaction frequency factor and reaction activation energy; x as a phenomenological quantity which controls sticking of oxygen adsorption on an Ir surface partially covered with CO and O; and dn_{CO_2}/dt as CO_2 rate, which was available through measurement.

Using experimentally measured (or set or given) quantities $\Phi=1.37\times10^{15}$ cm^{-2} s^{-1}, $n_{Ir}=1.56\times10^{15}$ cm^{-2}, $s_{CO}=1$, $\nu_{CO}=1\times10^{13}$ s^{-1}, $E_{CO}=140$ kJ/mol, $\nu_{rea}=10^5$ ML^{-1} s^{-1}, $E_{rea}=40$ kJ/mol, and $s_O=0.11$, by chosing $x=3$ [25] (and references therein), the essentials of the measured CO_2 rate versus Y dependence as shown in Fig. 1, including bistability, was reproduced in a very satisfactory manner. The origin of the bistability can be traced back to the setting $x=3$ in Eq. (2). This makes the above RKDEs system nonlinear and makes bistable behavior possible.

The CO_2 rate versus Y data like those shown in Fig. 1 were observed to be strongly affected by the time periods allowed for determination of the CO_2 equilibrium rates. This effect forced the long time periods used to collect the data shown in Fig. 1 and suggests that the omission of diffusion in the above system of RKDEs is inappropriate and must be replaced by reaction-diffusion kinetics differential equations (RDKDEs). Including diffusion terms in the above Eqs. (1) and (2) will make the surface concentrations of CO and O dependent on space and time and allow for demixing of the adsorbed species into islands by which the rather slow approach to equilibrium rates could be explained. It is clear that from solutions of the set of RKDEs this feature is not accessible, since the time is not controlled by a physical process in this approach (only entering in a ''mathematical'' manner for definition of time derivatives).

The aim of the present paper is an extension the previous solution of the RKDEs to RDKDEs by inclusion of diffusion, and, more importantly, an experimental and theoretical investigation of the consequences of application of a ''noisy'' Y to the measured CO_2 rates. It is clear that an approach to the latter objective requires a solution of the former problem. As noted, implementation of diffusion on the surface into the set of differential equations results in (x,y) spatially resolved concentrations $n_e(x,y,t)$, $n_{CO}(x,y,t)$, and $n_O(x,y,t)$, which are, however, not accessible in the present experiments,

which rely on the measurement of the CO_2 rate only, a space average on the sample surface.

II. EXPERIMENTAL METHODS

The experiments were carried out in an UHV system equipped with instrumentation for surface preparation (Ar ion gun), characterization (AES spectrometer), and manipulation (T control, CO and O_2 gas handling). As described in more detail in Ref. [25], the essential component of the system is a small differentially pumped UHV chamber attached to the main chamber. The small chamber comprises a doser tube on its center axis and a quadrupole mass spectrometer (QMS, Balzers 400) in its pumping line. CO and oxygen of the highest available purity (99.997 % and 99.9999 %, respectively) were delivered from pressurized cylinders through reducing valves and two mass-flow controllers (MFCs, MKS 200). After appropriate mixing the gas was supplied to the input of the doser tube and directed from its output end normally to the sample surface. Sample temperatures were regulated within 1/100 K. The primary gas flux Φ (CO + oxygen) was held constant throughout the measurements and monitored by a MKS Baratron, only its relative CO content Y was changed by appropriate programming of the MFCs. The gas flux (O_2, CO, CO_2) emitted from the Ir surface was mass-analyzed by the QMS after randomization at the walls of the small chamber. Due to differentially pumping of the small chamber, the recorded CO_2 signals are proportional to CO_2 rates.

According to the manufacturers specification, the computer controlled MFCs allowed regulation of Y for CO and $1-Y$ for oxygen within ± 0.001. The intrinsic random noise on Y and $1-Y$ introduced by the MFCs was also ± 0.001.

The data measured for the present work were collected with a new set of MFCs, which replaced those used in the previous study [24]. With the new MFCs the hysteresis was measured between $Y=0.135$ and $Y=0.155$, i.e., displaced by 0.01 to higher values as compared to the previous data (indicated by the dotted hysteresis in Fig. 1). In order to check for consistency, the new MFCs were exchanged and the position of the hysteresis was determined again. The position of the hysteresis remained unchanged, from which it was concluded that the new MFCs provide correct gas flows and that at least one of the old MFCs was outside of its specification (which cannot be verified in the present laboratory with the required precision).

The experiments were performed at constant temperature, $T=500$ K, and constant total flux, $\Phi_{total}=0.88$ ML/s. At the start of an experimental run, the MFCs were operated at some initial values Y_{ini} and $1-Y_{ini}$, e.g., $Y_{ini}=0$ (pure oxygen flux), or $Y_{ini}=1$ (pure CO flux). At a time $t_0=0$ the Y (CO fraction of Φ_{total}) and $1-Y$ (oxygen fraction of Φ_{total}) values were set to Y_0 and $1-Y_0$ by appropriate programming of the MFCs. The CO_2 rate $R(Y_0,t)$ was recorded as a function of time. Beginning from $t=t_1$ a noise ΔY_1 was superimposed on Y_0. The CO_2 rate $R(Y_0,\Delta Y_1,t-t_1)$ was recorded until the noise was changed to a new value ΔY_2 at $t=t_2$, and so on.

The noise components ΔY were produced after selection of a noise amplitude ΔY_{max} through generation of random numbers ΔY in the interval $(-\Delta Y_{max},\Delta Y_{max})$. A computed ΔY value was superimposed on the mean Y value, Y_0, for a time period of 3 s. Subsequently, a new ΔY value was applied for 3 s, and so on. The interval 3 s was chosen as the duration of a noise component ΔY since the response time of the MFCs was only 0.5 s.

The time dependent particle fluxes at the surface, $\Phi_{CO}(t)$ and $\Phi_{O_2}(t)$, delivered by the gas supply via the MFCs and the doser tube were affected not only by the response time of the MFCs, but also by the conductivity of the doser tube, and the pumping speed of the connected vacuum system. In the present experiments, through programming of the MFCs in the described manner the time-averaged CO and oxygen fluxes as measured with the QMS in the small chamber were very well described by Gaussian distributions centered at the mean fluxes $\Phi_{CO}=\Phi_{total,mean}Y_0$ and $\Phi_{O_2}=\Phi_{total,mean}(1-Y_0)$, e.g., $\Phi_{CO}\sim\Phi_{total,mean}Y_0\exp(-[(Y-Y_0)/\Delta\sqrt{2}]^2)$, with Δ as a characteristic width.

Using these procedures, two types of measurements were performed.

Influence of noise on the stability of the high and low rate branches. A specific Y value was set, inside or outside of the hysteresis. After the system had assumed its equilibrium rate, noise was applied with increasing amplitudes and the resulting CO_2 rates were measured as a function of time.

From these measurements it was intended to obtain the stability of the high and low rate branches with respect to the application of noise, in particular the noise amplitude at which the hysteresis disappears.

Influence of noise on the approach to equilibrium rates. Starting with some Y_{ini} value, typically 0 or 1, Y was changed to Y_0, either inside or just outside the hysteresis region, as depicted in Fig. 1, and a noise ΔY was applied simultaneously.

These measurements were suggested by the very slow (many hours) approach to the equilibrium CO_2 rate after Y had been changed to a new value. Since birth and decay of island structures were assumed to play a key role here, through application of noise the effect of a statistically varying primary gas flux on these features was investigated.

III. THEORETICAL METHODS

Starting point of our approach is not an atomistic description of chemical reactions, but rather a continuum approach. We stress that we are considering experimental surfaces, which are covered by about 10^{15} particles per cm^2. This approach for a very large particle number is therefore qualitatively different from a Monte Carlo approach. We also emphasize that spatiotemporal fluctuations in the concentrations of O and CO are included in our approach in the spirit of a continuum approximation.

To describe the effect of spatial variations and the formation of spatial (spatiotemporal) patterns, we modify the rate equations given in the preceding section by incorporating diffusion terms,

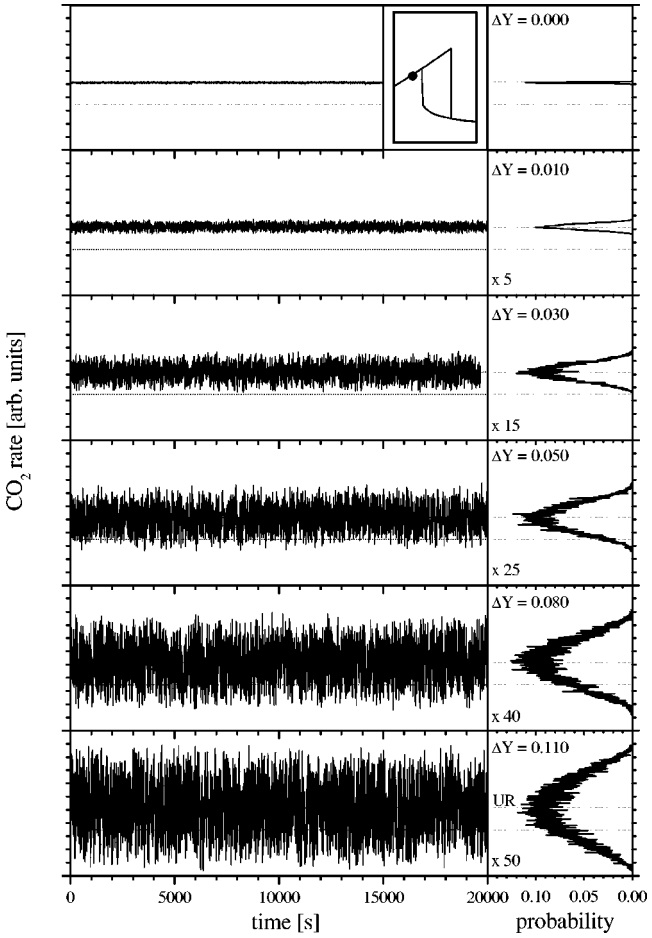

FIG. 3. Left panel: CO_2 rates measured as a function of time at $T=500$ K, $Y=0.130$, and various noise amplitudes ΔY. Right panel: normalized probability distributions of the rates in the left panel. Thin lines indicate the position of the upper and lower rate close to $Y=0.130$. The graph in the inset illustrates schematically the investigated point on the rate vs Y curve.

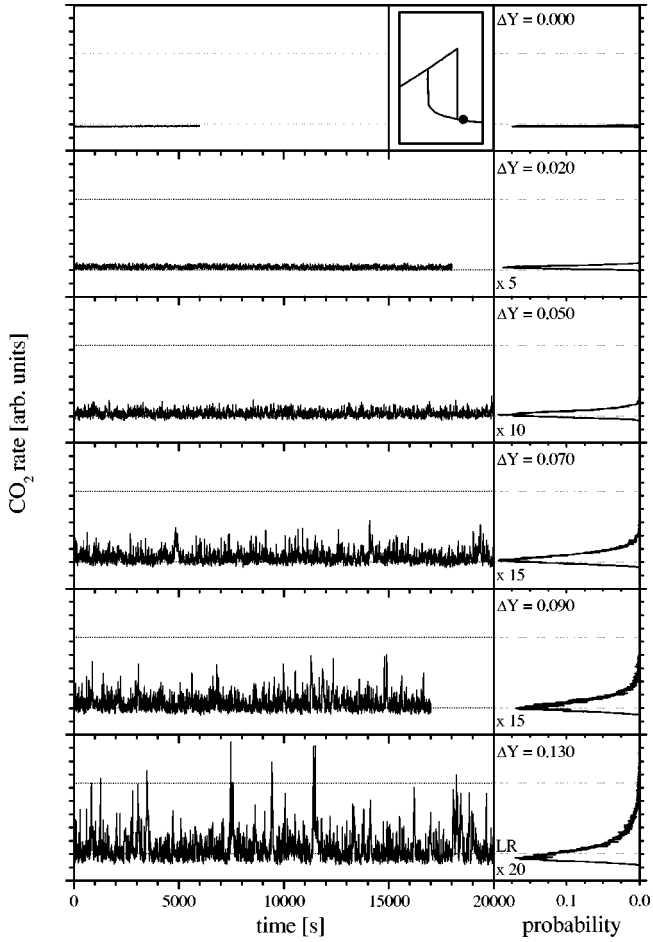

FIG. 4. Left panel: CO_2 rates measured as a function of time at 500 K, $Y=0.160$, and various noise amplitudes ΔY. Right panel: normalized probability distributions of the rates in the left panel. Other details as in Fig. 3.

$$\partial n_{\mathrm{CO}}/\partial t = s_{\mathrm{CO}}\Phi Y n_e/n_{\mathrm{Ir}} - \nu_{\mathrm{CO}} n_{\mathrm{CO}} \exp(-E_{\mathrm{CO}}/kT) - \nu_{rea} n_{\mathrm{CO}} n_{\mathrm{O}} \exp(-E_{rea}/kT) + D_{\mathrm{CO}}\nabla^2 n_{\mathrm{CO}}, \tag{4}$$

$$\partial n_{\mathrm{O}}/\partial t = 2 s_{\mathrm{O}}\Phi(1-Y)(n_e/n_{\mathrm{Ir}})^x - \nu_{rea} n_{\mathrm{CO}} n_{\mathrm{O}} \times \exp(-E_{rea}/kT) + D_{\mathrm{O}}\nabla^2 n_{\mathrm{O}}, \tag{5}$$

$$n_{\mathrm{CO}} + n_{\mathrm{O}} + n_e = n_{\mathrm{Ir}}, \tag{6}$$

where the last equation just reflects the fact that all Ir sites are either empty (n_e) or are occupied with CO (n_{CO}) or oxygen (n_{O}). For the parameters in Eqs. (4)–(6) we use the values $\Phi = 1.37\times 10^{15}$ cm^{-2} s^{-1}, $n_{\mathrm{Ir}} = 1.56\times 10^{15}$ cm^{-2}, $s_{\mathrm{CO}}=1$, $\nu_{\mathrm{CO}} = 1\times 10^{13}$ s^{-1}, $E_{\mathrm{CO}} = 140$ kJ/mol, $\nu_{rea} = 10^5$ ML^{-1} s^{-1}, $E_{rea} = 40$ kJ/mol, and $s_{\mathrm{O}} = 0.11$ and we choose $x=3$. These values coincide with those given in the preceding section. For the diffusion coefficients we estimate from the data collected in Ref. [26]: $D_{\mathrm{CO}} = 10^{-4}$ cm^2/s and $D_{\mathrm{O}} = 10^{-5}$ cm^2/s.

In Fig. 1(b) we have plotted the CO_2 rate as a function of the CO fraction for $T=500$ K obtained by numerically solving the differential equations (1)–(3). One clearly sees a fairly broad bistable region over which two values of the CO_2 rate are locally stable. It extends from $Y=0.084$ to $Y=0.131$. For sufficiently high and sufficiently low temperatures there is no hysteresis [24].

We would like to emphasize that we are making no adjustments and no rescaling to obtain the same location and width in order to achieve coincidence between the model and the experimental observations. As can be seen comparing Figs. 1(a) and 1(b) this implies a shift in the location of the hysteresis loop in Y as well as a smaller width for the experimental hysteresis loop when compared with the model.

To discuss the qualitative influence of noise on the CO fraction Y and, equivalently, on the oxygen fraction $1-Y$, we rewrite Eqs. (4)–(6) more compactly in the rescaled form

$$\partial n_{\mathrm{CO}}/\partial t = \alpha Y n_e - \beta n_{\mathrm{CO}} - \gamma n_{\mathrm{CO}} n_{\mathrm{O}} + D_{\mathrm{CO}}\nabla^2 n_{\mathrm{CO}}, \tag{7}$$

$$\partial n_{\mathrm{O}}/\partial t = \delta(1-Y) n_e^3 - \gamma n_{\mathrm{CO}} n_{\mathrm{O}} + D_{\mathrm{O}}\nabla^2 n_{\mathrm{O}}, \tag{8}$$

$$n_e = n_{\mathrm{Ir}} - n_{\mathrm{O}} - n_{\mathrm{CO}}. \tag{9}$$

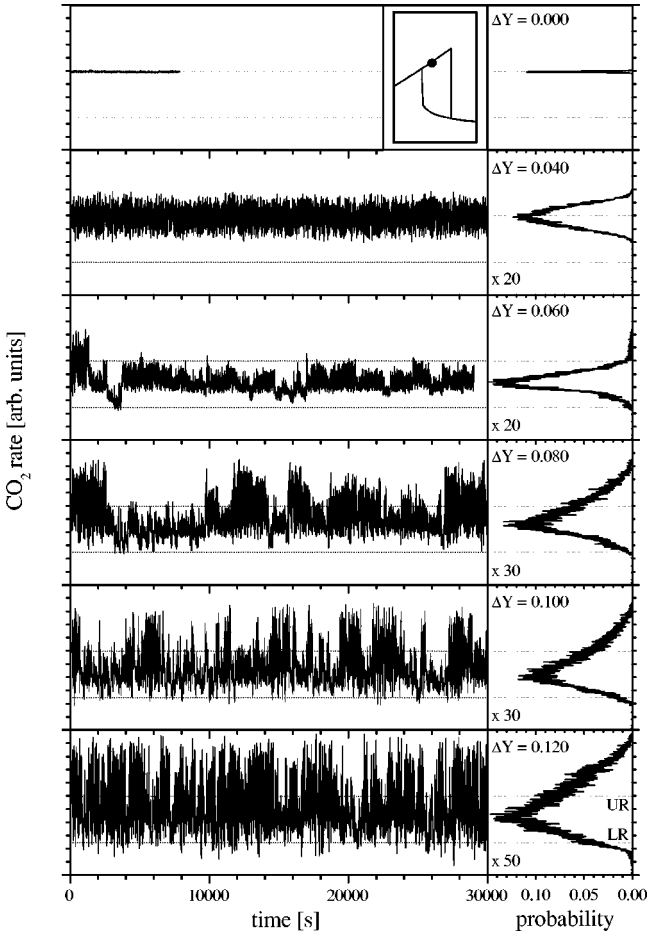

FIG. 5. Left panel: CO_2 rates measured as a function of time at 500 K, $Y=0.142$ (upper rate), and various noise amplitudes ΔY. Right panel: normalized probability distributions of the rates in the left panel. Other details as in Fig. 3.

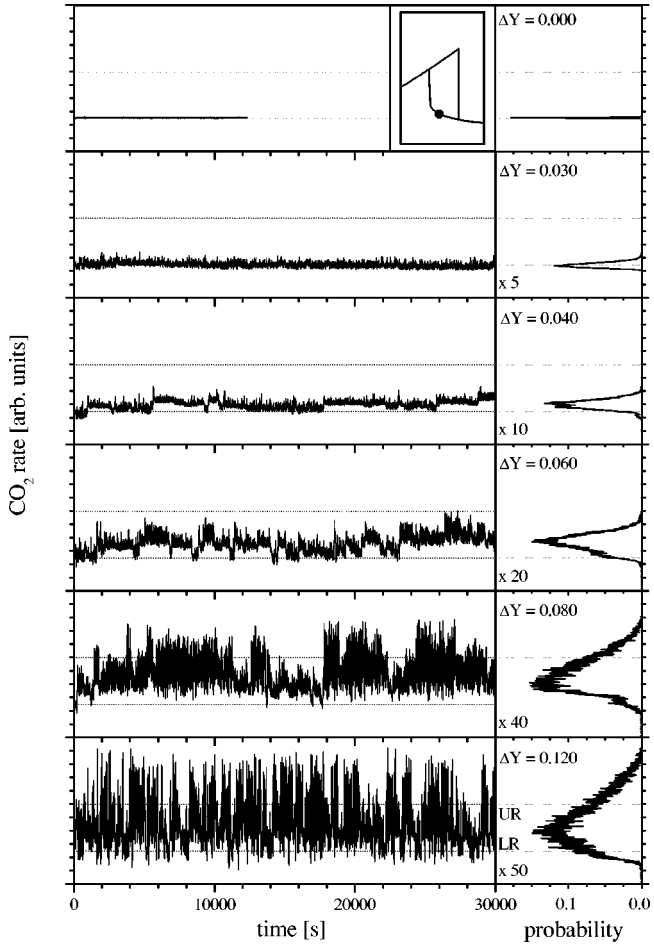

FIG. 6. Left panel: CO_2 rates measured as a function of time at 500 K, $Y=0.142$ (lower rate), and various noise amplitudes ΔY. Right panel: normalized probability distributions of the rates in the left panel. Other details as in Fig. 3.

If we now superpose noise on Y,

$$Y \rightarrow Y + \xi, \tag{10}$$

we obtain for the first equation an additive noise term $\sim \alpha n_{\mathrm{Ir}} \xi$ and a multiplicative noise term $\sim -\alpha(n_{\mathrm{O}}+n_{\mathrm{CO}})\xi$. For the second equation the noise terms take the form $-\delta(n_{\mathrm{Ir}}-n_{\mathrm{O}}-n_{\mathrm{CO}})^3\xi$ consisting again of an additive part $\sim -\delta n_{\mathrm{Ir}}^3 \xi$ and a multiplicative part $\sim -[(n_{\mathrm{O}}+n_{\mathrm{CO}})^3 + 3n_{\mathrm{Ir}}(n_{\mathrm{O}}+n_{\mathrm{CO}})^2 - 3n_{\mathrm{Ir}}^2(n_{\mathrm{O}}+n_{\mathrm{CO}})]\xi$.

Thus one has contributions from both types of noise. Such stochastic processes have been discussed in Ref. [13] for the case of Gaussian white noise in spatially homogeneous systems using the Fokker-Planck approach. However, since the type of noise studied in our experiments is of a different nature and since we investigate as well the effect of spatial variations, we solve the resulting Langevin equations directly numerically. For our numerical calculations we use a time-splitting method and second-order finite differencing for the diffusion term. We have varied the box length (lateral dimension of box size in two dimensions) from $L=10$ to $L=40$ ($L=2$ to $L=10$ in two dimensions) and use a grid size of $dx=0.0125$ in one spatial dimension and $dx=dy=0.0125$ in two spatial dimensions. For the time step we used $dt=0.01$. We checked that our choices for the grid size and the time step did not influence the results obtained, by varying both, the grid size and the time step. For all numerical solutions of Eqs. (4)–(6) the noise ξ [with the properties $\langle \xi \rangle = 0$ and $\langle \xi(x,t)\xi(x+dx,t+dt)\rangle = Q\delta(dx)\delta(dt)$] was applied at all times and was varying in space—compare also the discussion in the next paragraph for additional details of the implementation. Only if one would start with a spatially homogeneous state and would apply strictly spatially homogeneous noise, the terms involving the Laplace operator would vanish. We would like to stress, however, that the noise term $\sim \xi$ in Eq. (10) varies as a function of space and time.

To obtain results that can be compared to the experiments, we averaged the applied noise over a spatial interval of $\Delta x = 0.125$ in one dimension and over $\Delta x = 0.25, \Delta y = 0.25$ in two spatial dimensions. This procedure accounts for the fact that the concentration of O and CO particles on the surface is not homogeneous. Accordingly effective sticking coefficients vary as a function of space and time. In addition, we averaged the applied noise over a time period $\tau_{noise}=9$ s. This time scale was chosen to account for the experimentally ob-

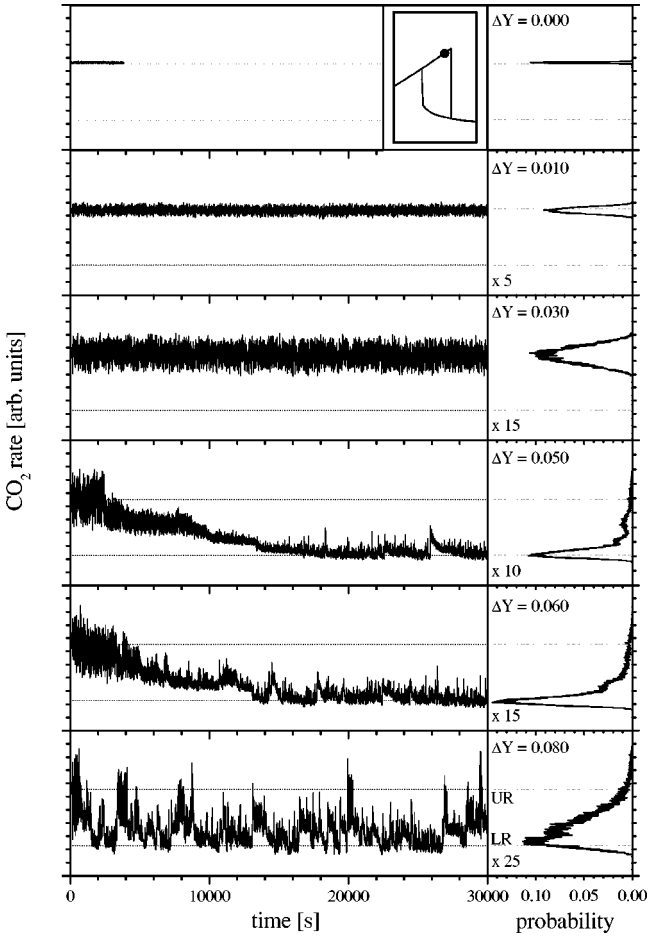

FIG. 7. Left panel: CO_2 rates measured as a function of time at 500 K, $Y=0.150$ (upper rate), and various noise amplitudes ΔY. Right panel: normalized probability distributions of the rates in the left panel. Other details as in Fig. 3.

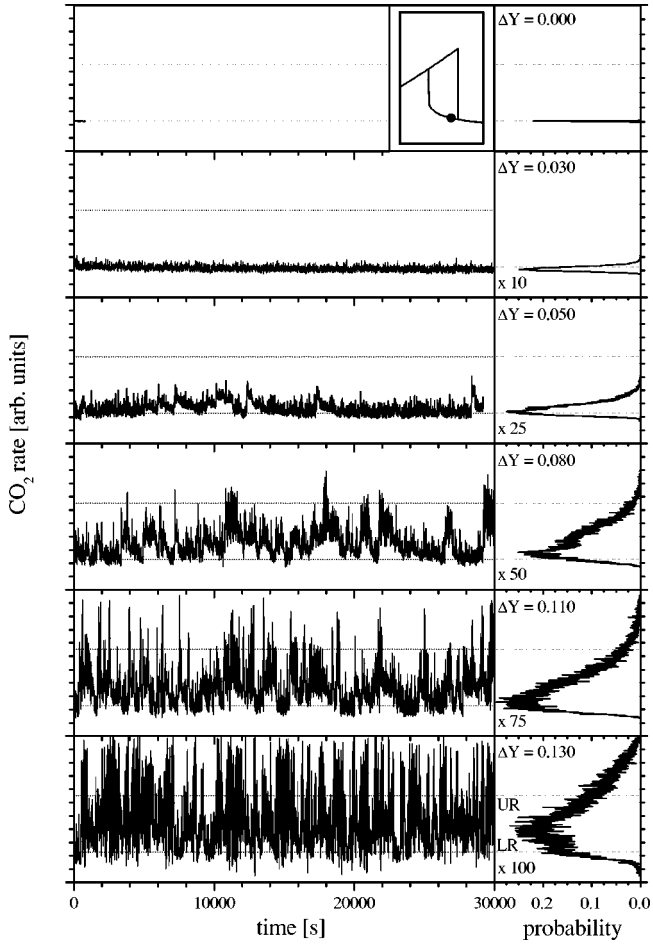

FIG. 8. Left panel: CO_2 rates measured as a function of time at 500 K, $Y=0.150$ (lower rate), and various noise amplitudes ΔY. Right panel: normalized probability distributions of the rates in the left panel. Other details as in Fig. 3.

served phenomenology for short times. This averaging time was fixed once and kept constant for all runs to provide/guarantee a coherent theoretical picture not influenced by parameter variations. Compare the discussion further below for the details about the comparison to the experimental results.

IV. RESULTS

In the course of the measurements the time dependent CO_2 rates $R(t)$ were recorded at about a dozen points in the (R,Y) diagram shown in Fig. 1, with Y varied between $Y=0.1$ and $Y=0.2$, at up to ten noise amplitudes varying between $\Delta Y_{max}=0$ and $\Delta Y_{max}=0.2$. Including reproducing measurements the collected data set consists of more than 100 CO_2 rate versus time curves, typically measured for several hours each, at a data taking frequency of about 1 Hz. Clearly, only a representative selection of these data can be presented here. In order to provide information about the essential consequences of noise application on the surface reaction, seven characteristic examples were selected, two just outside and four inside of the hysteresis region, and one example of the consequences of noise on the approach to stationary rates. For easier reading, the figures shown below contain a small graphical annotation which allows an easy orientation concerning the position of the investigated point in the CO_2 rate/Y diagram. The figures provide the time evolution of the CO_2 rates R at selected $Y_0, \Delta Y_{max}$ settings and the normalized probability distributions of $R(t)$. For the latter, dotted lines are included to provide the position of the upper (R_{up}, UR in the figures) and lower (R_{low}, LR in the figures) rates at or close to the chosen Y value. Furthermore, instead of using ΔY_{max} for specification of the noise amplitude, the shorthand notation ΔY applies below. Lastly, the ΔY values given below do not include the intrinsic noise of the MFCs, but only that noise which was applied intentionally.

A. Noise applied outside the hysteresis regime

Figure 3 displays CO_2 rates measured at $Y_0=0.13$ at increasing noise amplitudes. Consulting Fig. 1 it is seen that with this choice of Y the system is initially placed on the upper rate branch just below the onset of the hysteresis region. In the left panel of Fig. 3 the raw CO_2 rates $R(t)$ are shown as a function of time, with $t=0$ an arbitrary time,

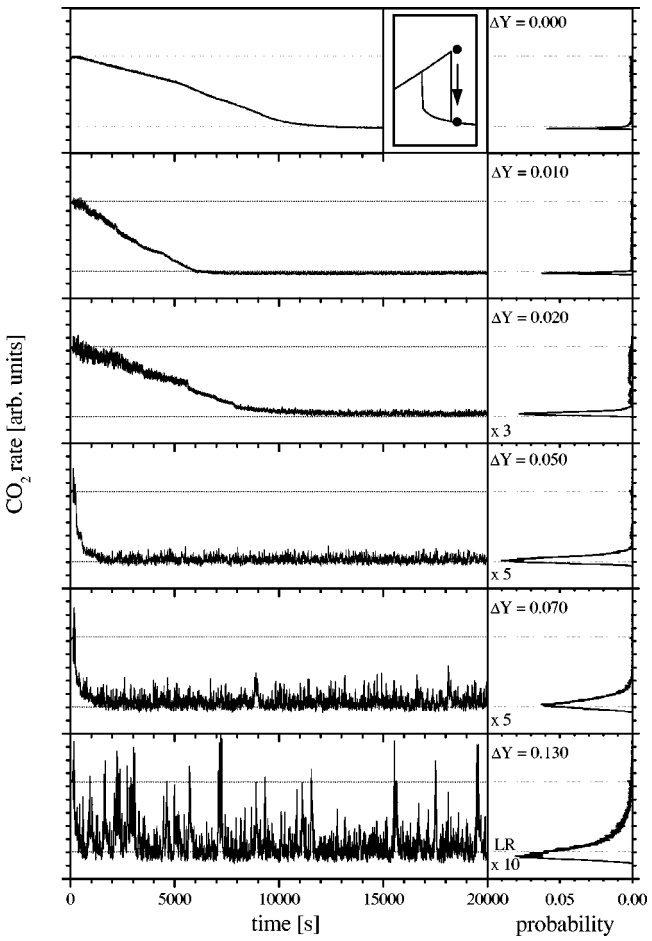

FIG. 9. Left panel: CO_2 rates measured as a function of time at 500 K, $Y=0.160$ (upper rate), and various noise amplitudes ΔY. Right panel: normalized probability distributions of the rates in the left panel. Other details as in Fig. 3.

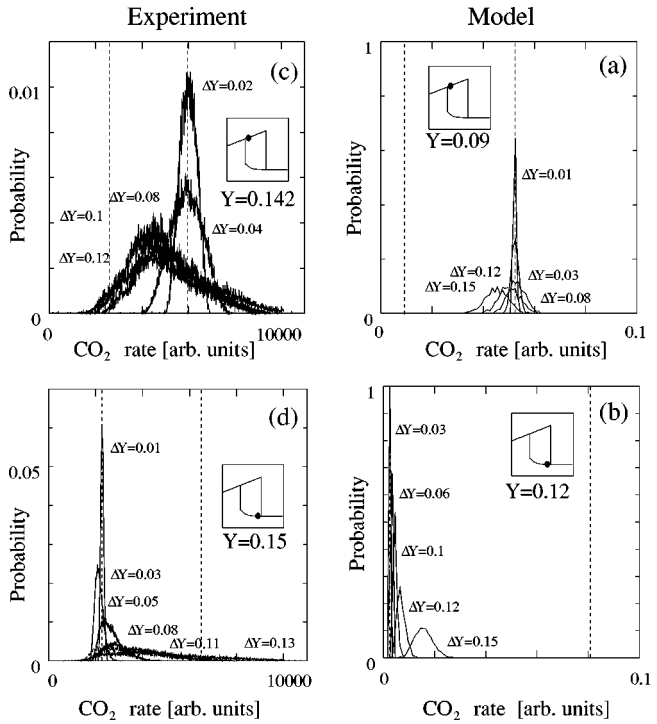

FIG. 10. The probability densities are plotted for the upper and lower branch as a function of noise strength ΔY. The box size is $L=10$, the averaging interval for the noise $\Delta x=0.125$, the grid size $dx=0.0125$, the time step $dt=0.01$, and the averaging time for the noise, $\tau_{noise}=9$ s. (a) Probability density on the upper branch for five values $\Delta Y=0.01$, 0.03, 0.08, 0.12, and 0.15 for the noise strength and $Y=0.09$. We note that the probability density broadens first and that then the peak also shifts towards the lower branch. (b) Probability density on the lower branch for five values $\Delta Y=0.03$, 0.06, 0.10, 0.12, and 0.15 for $Y=0.12$. In this case the peak of the probability density also broadens but starts to shift towards the upper branch immediately as the noise strength is increased. (c) and (d) show the experimental analogs using the experimental results presented in Figs. 5 and 8. Note that no parameter adjustments are made to achieve agreement between experiment and theory at the same Y value (compare the detailed discussion in Sec. III).

selected at the end of transient CO_2 rate versus time behavior after installation of Y_0 *without* applied noise. From the time scale supplied at the abscissa it is clear that the $R(t)$ data shown correspond to long lasting effects and not to short transient phenomena caused by switching from Y_{ini} to Y_0 at the start of the experiment. In the right panel of Fig. 3 the normalized probability distributions $P(R)$ of these rates are shown. With no external noise ($\Delta Y=0$) applied to Y, the CO_2 rate $R(t)$ exhibits a small noise. The related probability distribution $P(R)$ has a sharp peak centered at the upper rate R_{up}, the stationary CO_2 rate at $Y=0.13$. Ideally, at $\Delta Y=0$ the $P(R)$ distribution should be a δ-function at R_{up}. Note, however, that the MFCs exhibit a combined internal noise component with $\Delta Y=0.002$, which prohibits a δ-function like appearance of $P(R)$. Accordingly, the topmost curves in Fig. 3 characterize the low- (zero external) noise limit accessible with the present instrumentation.

It is seen in the left panel of Fig. 3 that with increasing external noise amplitude ΔY the CO_2 rates exhibit higher noise, also reflected in the corresponding $P(R)$ distributions in the right panel. These distributions get wider, however they stay centered at R_{up}. The shape of the $P(R)$ distributions reflects the distribution of noisy Y values applied. Note that even at noise amplitudes sufficient to shift the system fully into the hysteresis region, the center of the probability distributions of the rates does not shift away from R_{up} or develop a second peak. At $Y=0.13$ the rates R just fluctuate around the upper rate R_{up}, which might be expressed by saying that at $Y=0.13$ the system is located in a potential minimum at (Y,R_{up}) and is very stable against application of noise.

Figure 4 shows CO_2 rates measured at $Y=0.16$, i.e., just above that of the hysteresis region, with increasing noise amplitudes. As seen in Fig. 1, at this Y value the stability point of the system is located on the (nonhysteretic) lower rate branch. With intrinsic MFC noise only the $P(R)$ distribution has a sharp peak at R_{low}. $P(R)$ develops a wing towards higher rates through application of noise, but drops off sharply towards lower rates. This is required since less than the minimum rate is not possible. At the highest noise amplitude, $\Delta Y=0.13$, there are sharp rate peaks in the $R(t)$ curve which even pass the upper rate determined just at the

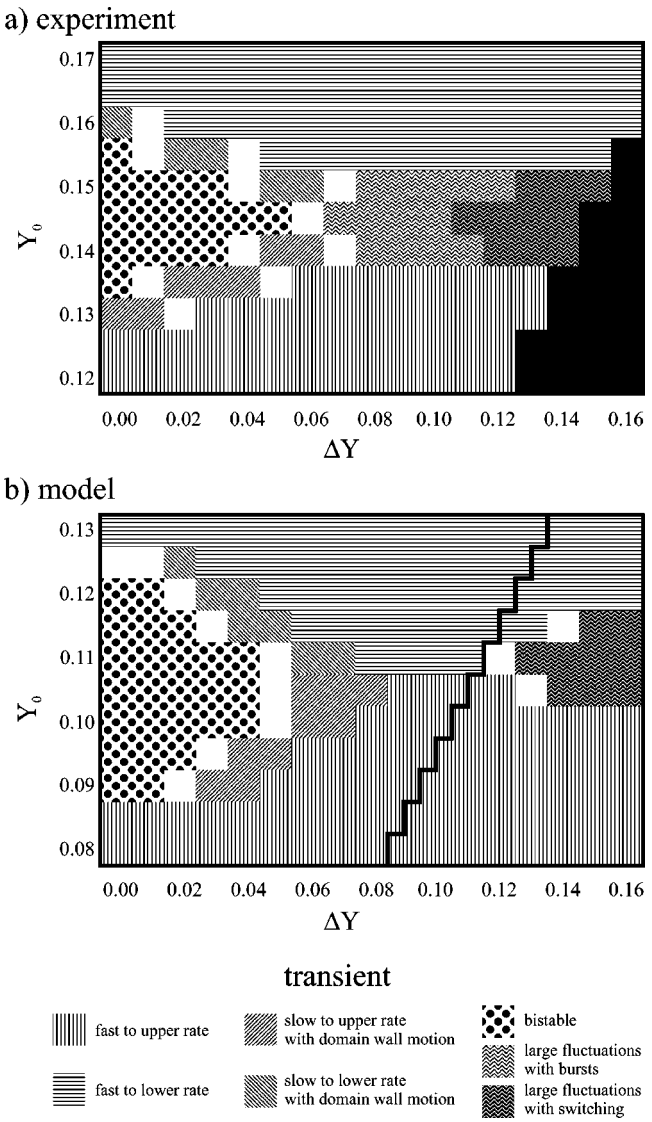

FIG. 11. Phase diagram showing the transient behavior: (a) experimental and (b) model. The phenomena occurring are plotted in the Y vs noise strength ΔY plane. We observe, in the deterministically bistable regime, transitions from the upper to the lower branch (indicated by horizontal lines), from the lower to the upper branch (vertical lines), bistability, domain wall motion in the long-time limit ($t=10^4-10^5$ s) from the lower to the upper branch (lines tilted by 45°) and from the upper to the lower branch (lines tilted by $-45°$), and noise-induced switching (wavy lines). The white areas denote regions for which a clear-cut assignment to one type of behavior was not possible. The black region cannot be reached experimentally.

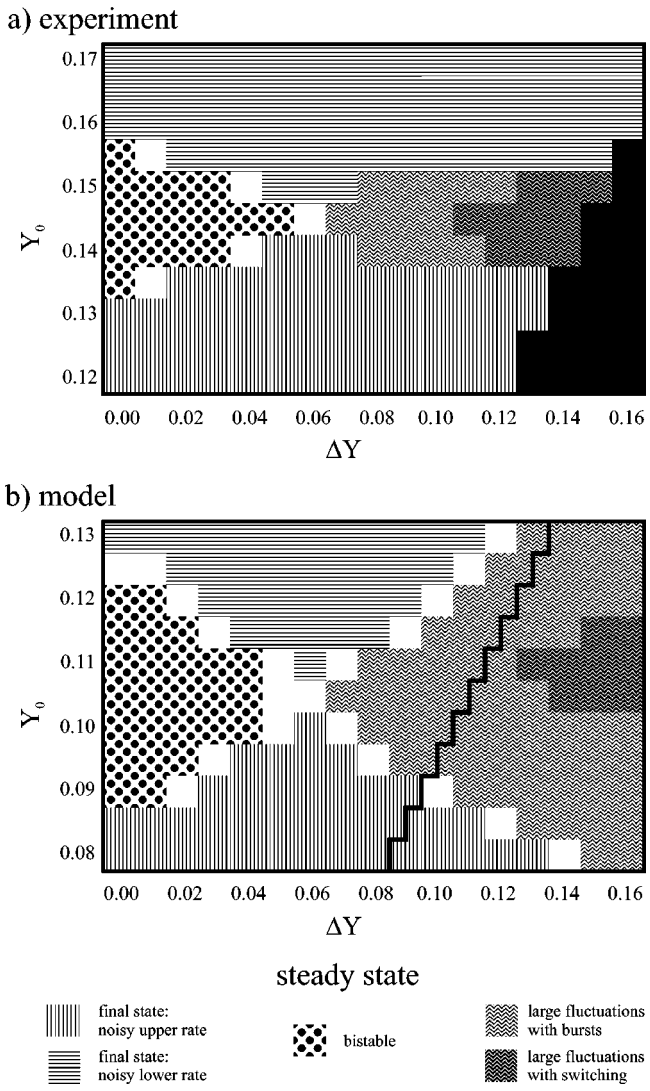

FIG. 12. Phase diagram showing the phenomena obtained in the long-time limit $t\to\infty$: (a) experimental and (b) model. The types of characteristic behavior include lower branch with noise superposed (horizontal lines), upper branch with noise superposed (vertical lines), bistable behavior, and—for large values of the noise strength—switching and bursts (wavy lines). Other details are as in Fig. 11.

hysteresis border. This phenomenon is due to the fact that at this high noise amplitude it can happen that one pure oxygen noise pulse covers the surface with oxgen and a subsequent CO-rich noise pulse causes a rate which is not achieved under steady state conditions. The distribution of the high peaks in the bottom of Fig. 4 qualifies these events as rare, as expected. In spite of these transients the rate distributions illustrate that at $Y=0.16$ the system is located in a potential minimum at (Y,R_{low}) and application of noise does not shift it out of that minimum.

B. Noise applied inside the hysteresis regime

The data shown in Fig. 5 were taken starting at the upper branch of the hysteresis at $Y=0.142$, close to, but below the center of the hysteresis. Without external noise applied, the probability distribution $P(R)$ is a sharp peak centered at R_{up}. Application of a small noise amplitude $\Delta Y=0.04$ only broadens $P(R)$, like that observed in Fig. 3, but at $\Delta Y=0.06$ further broadening is accompanied by a shift of its maximum away from R_{up} towards R_{low}. At larger ΔY values the distribution gets wider, its maximum shifts to a rate close to midway between R_{up} and R_{low}, but there are still significant contributions from rates around R_{up}. If the starting point was selected also at $Y=0.142$ but at the lower rate R_{low}, as was done for collection of the data shown in Fig. 6, the maximum of $P(R)$ shifts away from R_{low} already at

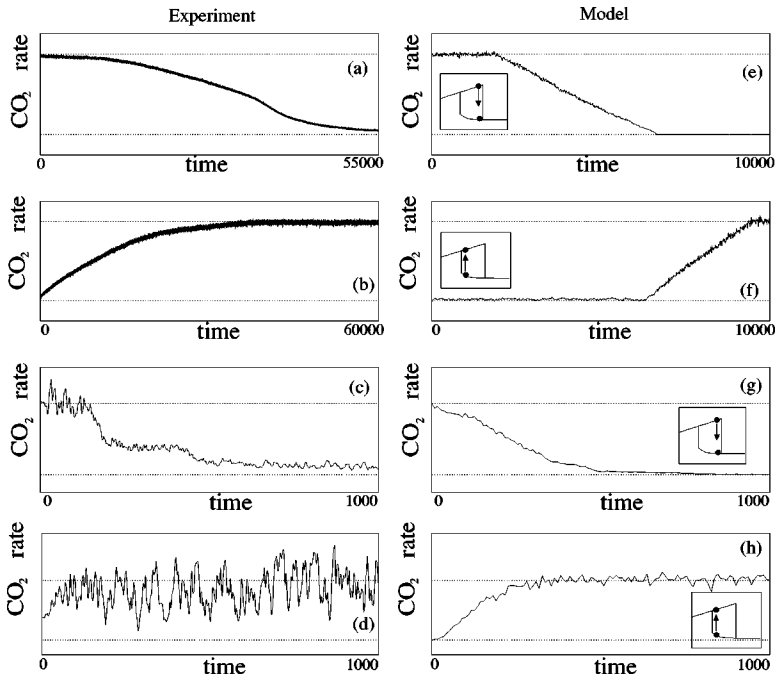

FIG. 13. The time dependence of the CO_2 rate is shown for slow and fast transitions from the upper to the lower branch and vice versa. Slow transition from upper to lower branch: (a) $Y=0.16$, $\Delta Y=0$; (e) $Y=0.12$ and $\Delta Y=0.027$. Slow transition from lower to upper branch: (b) $Y=0.13$, $\Delta Y=0$; (f) $Y=0.09$ and $\Delta Y=0.025$. Fast transition from upper to lower branch: (c) $Y=0.16$, $\Delta Y=0.05$; (g) $Y=0.12$ and $\Delta Y=0.06$. Fast transition from lower to upper branch: (d) $Y=0.13$, $\Delta Y=0.05$, (h) $Y=0.09$ and $\Delta Y=0.06$. Note that the time scale on the abscissa is different by an order of magnitude when going from (e) and (f) to (g) and (h). Time t is in seconds and the CO_2 rate in arbitrary units.

$\Delta Y=0.04$. Through increased noise amplitudes the shift gets larger and the distribution $P(R)$ broadens. At $\Delta Y=0.08$ and 0.12 the maximum of $P(R)$ is located midway between R_{up} and R_{low} and a large fraction of $P(R)$ is located around R_{up}. Apparently, states of the system which lead to rates at or close to R_{up} are more stable in the long-time limit (compare Figs. 5 and 6, especially for $\Delta Y=0.04$) with respect to application of noise than those which lead to rates near R_{low}. In terms of the double-well potential picture for the description of bistability one would conclude that close to but below the center of the hysteresis the state (Y,R_{up}) defines the deeper well and the state (Y,R_{low}) the less deep well.

Moving within the hysteresis region a little upwards and beyond the hysteresis center by choosing $Y=0.15$ and starting at the upper rate R_{up} the rates and probability distributions shown in Fig. 7 were obtained. Without applied noise and noise amplitudes of 0.01 and 0.03 the features are as expected from the previous examples. However, at a noise amplitude of $\Delta Y=0.05$ the system at first exhibits substantial rate fluctuations around R_{up} for about 4000 s. Then, while still fluctuating, the rate drops in a large time period of several thousand seconds until it settles with smaller fluctuations close to the lower rate R_{low}. The probability distribution for $\Delta Y=0.05$ reflects this behavior by a strong peak at R_{low} and weaker features between R_{low} and R_{up}. Application of a noise amplitude of $\Delta Y=0.06$ causes the same effects, although a little accelerated. At $\Delta Y=0.08$ the CO_2 rate drops in a noisy fashion within less than 2000 s to R_{low} and its asymptotic development with time exhibits strong fluctuations around R_{low} with a probability distribution which drops off towards low CO_2 rates due to the low rate limitation considered above. The reaction of the system to noise illustrates that at $Y=0.15$ the state which corresponds to R_{up} is fairly unstable and that application of a sufficiently large noise drives the system into the state which corresponds to the low rate R_{low}. Accordingly, the state (Y,R_{up}) is in the shallower potential well and the state (Y,R_{low}) in the deeper well.

The response of the system to noise prepared at $Y=0.15$ in the lower rate at R_{low} is illustrated in Fig. 8. Without noise and for small noise amplitude the rates and rate distributions are expected in view of the previous examples. The small downward shift of the whole probability distribution for $\Delta Y=0.03$ is within experimental accuracy for these long measurements. At noise amplitudes $\Delta Y=0.05$ and 0.08 the rate distributions $P(R)$ develop a wing towards R_{up}, but the maximum of the distribution stays at or close to R_{low}. A comparison with Fig. 7 illustrates that at these noise amplitudes the system prepared initially in the upper rate R_{up} moves to the lower rate R_{low}. Application of even higher ΔY values causes further broadening of $P(R)$ at $\Delta Y=0.08$ and finally at $\Delta Y=0.13$ a substantial shift of the maximum of $P(R)$ away from R_{low}. A consistency check of the data can be performed by comparing the rates and probability distributions for $\Delta Y=0.08$ in Figs. 7 and 8. It is seen that the curves are not identical, as required by the use of random noise, but exhibit the same essential features. From Fig. 8 one can conclude that the system at $Y=0.15$ in the state

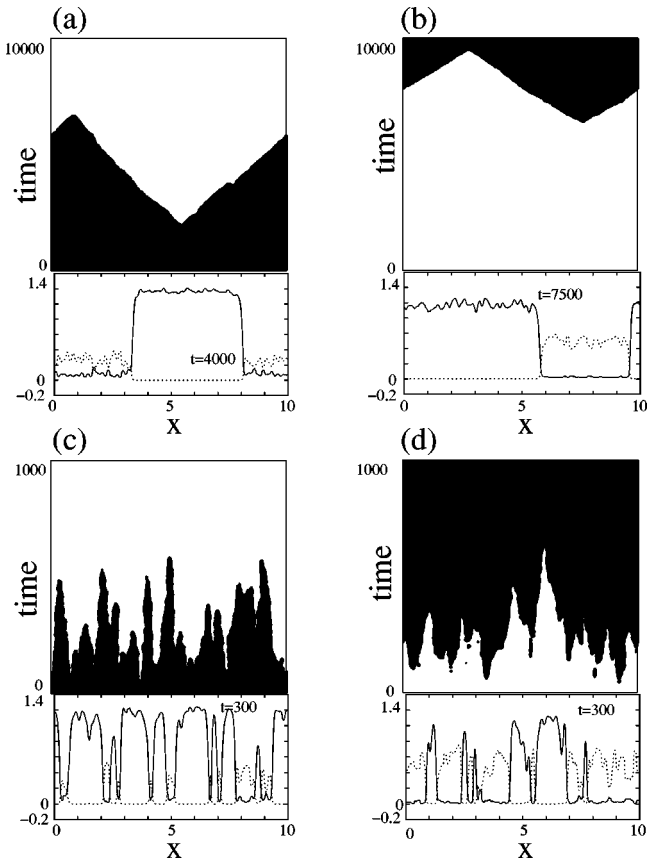

FIG. 14. Space-time plots and snapshots of the spatial structure for a fixed time t for the transitions described in Fig. 13. We have plotted in black all values for n_{CO} which satisfy $n_{\mathrm{CO}}<1/2(n_{\mathrm{CO}}^{upper}+n_{\mathrm{CO}}^{lower})$, where n_{CO}^{upper} and n_{CO}^{lower} are taken from the bistable solutions of the ordinary differential equations. The solid line indicates the concentration of CO and the dashed line that of O. The times t of the snapshots are (a) $t=4000$, (b) $t=7500$, (c) $t=300$, and (d) $t=300$. We note that (a) and (b) show that the long transients are dominated by the slow motion of a small number of domain walls while the short transients displayed in (c) and (d) are associated with a rapidly varying spatial structure. The time on the ordinates is in seconds and the abscissa is in scaled length units.

which corresponds to R_{low} is fairly stable and that even application of large noise does not drive the system away from that state. This confirms the above conclusion that at $Y=0.15$ the absolute minimum of the double-well potential of the bistable system is located at (Y,R_{low}).

C. Approach to stationary, possibly noisy rates

In the experimental section it was specified that preceding application of noise the procedure to install a starting point of an experiment at Y_0 consisted of changing Y from an initial Y_{ini} (e.g., $Y_{ini}=0$) value to the required Y_0 value. Since the response time of the MFCs is about 0.5 s, long-time transients of the CO_2 rate for approach to the stationary state could be measured. Examples of these measurements are shown in Fig. 9. The initial procedures for these measurements were identical: $Y_{ini}=0$, $\Delta Y_{ini}=0$, installation of $Y_0=0.16$ while keeping $\Delta Y=\Delta Y_{ini}$, application of a required ΔY at $t=120$ s (a time arbitrarily chosen, but sufficiently long to guarantee that the rate is constant before the noise is applied). The fact that the approach to equilibrium is faster for $\Delta Y=0.01$ than for $\Delta Y=0.02$ probably reflects inevitable variations in the initial conditions although the preparation of the initial state was identical. It is seen in Fig. 9 that with $\Delta Y=0$ the CO_2 rate R initially assumes a value close to R_{up}, close to the upper rate of the nearby hysteretic state at $Y=0.155$, then creeps slowly down to R_{low}, which is close to the lower rate of the adjacent hysteretic state. The probability distribution reflects this behavior: during most of the time covered by Fig. 9 the system had settled in the lower rate state at R_{low}. Application of noise changes the phenomena significantly. The approach to the more stable state at R_{low} gets faster and the CO_2 rates recorded during and after the transition exhibit noise. It is seen from Fig. 9 that the acceleration of the approach to the stationary (and noisy) state R_{low} by application of sufficiently large noise, $\Delta Y=0.13$, is so fast that it occurs within the first few 100 s after application of the noise.

D. Noise effects observed in the numerical investigations

In Fig. 10 we plot the probability densities for the upper and lower branch as a function of noise intensity. The dotted lines on the abscissa indicate the locations of the upper and lower branch in the noise-free case. As one expects intuitively, the probability density broadens as the noise strength increases in both cases. However, it is worthwhile to note that for the upper branch the probability density broadens first before the peak starts to shift towards the lower branch [Fig. 10(a)], while for the lower branch the shift process sets in as soon as noise is superposed [Fig. 10(b)]. A comparison with the experimental data presented in Figs. 10(c) and 10(d) illustrates that the essential features of the experimental data are reproduced by the theoretical model almost quantitatively.

In Fig. 11 we present the phase diagrams showing the transient behavior obtained from the experiment [Fig. 11(a)] and the model [Fig. 11(b)]. In the diagrams we plot the characteristics of the system arranged in $(Y,\Delta Y)$ fields classified according to different types of behavior. The classification is described in detail at the bottom of the figure. Outside the bistable regime we observe noisy behavior on the stable branch, that is, on the upper branch for small values of Y and on the lower branch for large values of Y. In the bistable regime a rich variety of behaviors is observed as the noise strength is increased. There is bistability for sufficiently small noise strength: the system stays on the upper or lower branch when noise is applied. There is domain wall motion leading to very long transients of 10^4–10^5 s (compare also the discussion further below), and there are noise-induced transitions from the upper to the lower or from the lower to the upper branch for intermediate noise strength and finally noise-induced switching between the two branches for sufficiently high noise strength.

In Fig. 12 the results obtained in the long-time limit $t\rightarrow\infty$ are displayed complementing the transient behavior shown in Fig. 11 and classified accordingly. As expected, one

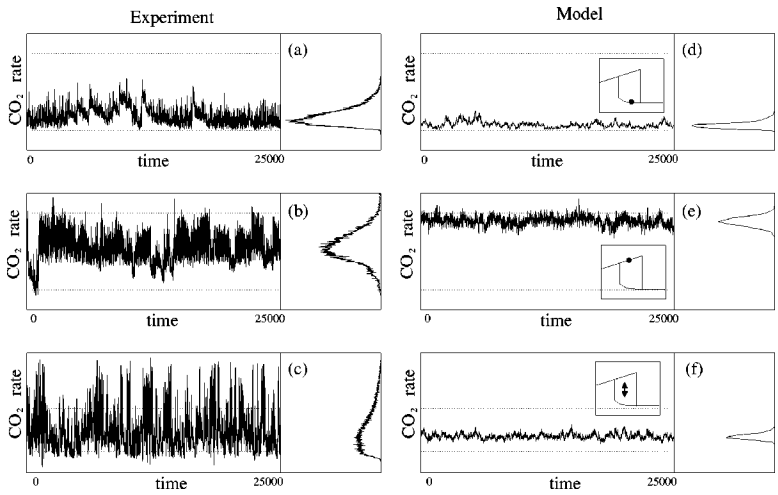

FIG. 15. The time dependence of the CO_2 rate is shown for the lower and upper branch with bursts and for noise-induced switching. Lower branch with bursts: (a) $Y=0.15$, $\Delta Y=0.05$, (d) $Y=0.11$ and $\Delta Y=0.09$. Upper branch with bursts: (b) $Y=0.142$, $\Delta Y=0.06$; (e) $Y=0.105$ and $\Delta Y=0.08$. Noise-induced switching: (c) $Y=0.145$, $\Delta Y=0.13$; (f) $Y=0.11$ and $\Delta Y=0.13$. These types of behavior persist in the long-time limit $t\rightarrow\infty$. The graphs in the right column show the probability density of CO_2. We note that the averaging time chosen for the modeling is three times longer than that for the experimental runs. Correspondingly the variations in CO_2 in the left column are larger and more rapid. A smaller averaging time in the modeling also leads to larger and more rapid variations. Time t is in seconds and the CO_2 rate in arbitrary units.

finds outside the deterministically bistable regime noisy behavior on the upper and lower branch, respectively. Inside the bistable regime in the noise-free state, we have with increasing noise strength bistable behavior, bursts, and finally noise-induced switching for high noise strength, a phenomenon that continues indefinitely—a feature that also applies to the bursts.

After we have given the overview over the various types of behavior observed, we will now present in detail the characteristic features of each type. In Fig. 13 we have plotted the time dependence of the CO_2 rate for fast and slow transitions from the upper to the lower branch and vice versa. We note that the difference in the time scales involved in these transitions can vary by more than two orders of magnitude. The origin of these differences becomes clear when the spatiotemporal behavior is investigated. In Fig. 14 we show space-time plots and snapshots of the spatial structures for the transitions presented in Fig. 13 obtained from one-dimensional (1D) simulations. We note that the speed of domain wall motion is smaller, when the parameter value of Y is taken closer to $Y=0.109$, where the speed of wall motion is zero. One clearly sees the qualitative differences in behavior between the long transients associated with domain wall motion and the short transients for which one has mainly small and irregular sized domains of the unstable type vanishing fairly rapidly as they are replaced by the more stable state. Finally we emphasize that the duration of the initial plateaulike region for the transitions with long transients depends sensitively on the initial conditions of the noise. Qualitatively very little changes when the numerical simulations are performed for two spatial dimensions instead of one spatial dimension (compare also the discussion of the results for our numerical simulations in two spatial dimensions below).

In Fig. 15 we show the time dependence of the CO_2 rate for the lower and upper branch with bursts as well as for the noise-induced switching. On the right side of each type of time dependence the associated probability distribution is displayed. All three types of behavior continue indefinitely as long as the noise is supplied. When the noise is turned off the system returns to the scenario expected from the analysis of the purely deterministic system. In Fig. 16 we have assembled space-time plots and snapshots of the spatial patterns for the scenarios shown in Fig. 15 obtained from 1D simulations. One clearly sees the small spatial scales (high wave-vector contents) connected with noise-induced bursts as well as with noise-induced switching. In all three cases this is brought out very clearly by both, the space-time plots and the snapshots, while these types of behavior appear not as dramatic when only the spatially averaged temporal behavior is considered (compare Fig. 15 for an instructive contrast).

In Figs. 17 and 18 we present two examples of the spatiotemporal dynamics obtained from two-dimensional simulations. In Fig. 17 the long transient from the upper to the lower branch is shown for a box size of $L\times L=2\times 2$. The times at which the six two-dimensional snapshots are taken are indicated by arrows in the temporal evolution of CO_2 shown on top in Fig. 17. One clearly sees that the transition occurs via nucleation followed by a slow domain wall motion. It would surely be very interesting to check this prediction by experiments with spatial resolution like those using photoelectron emission microscopy. In Fig. 18 we show an example of the burst behavior for bursts occurring superposed on the lower branch. The two snapshots show a significant change in the spatial pattern when the bursts occur [Fig. 18(b)].

V. DISCUSSION

For values of the parameters Y for which there is deterministically only one basin of attraction (Figs. 3 and 4), the

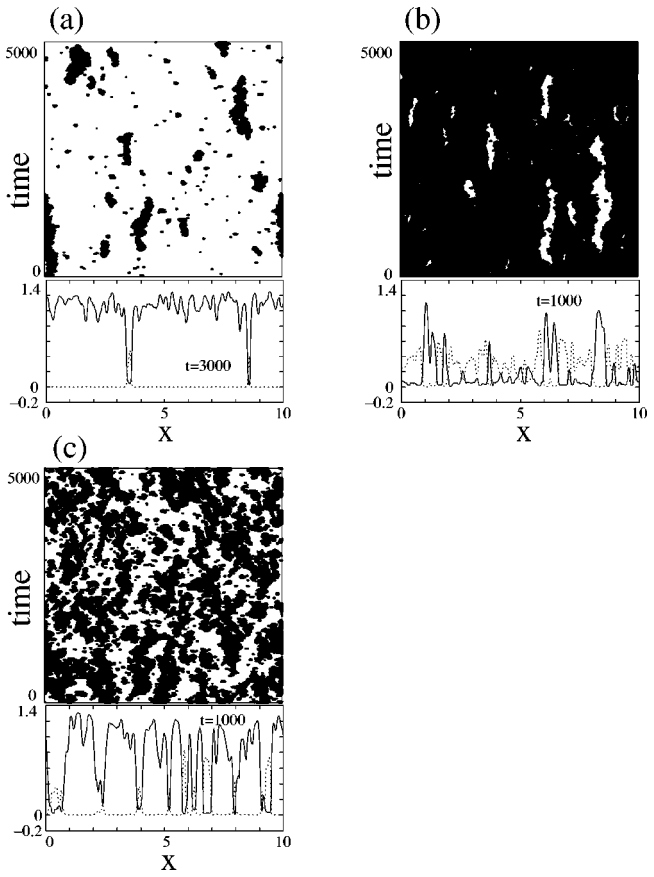

FIG. 16. Space-time plots and snapshots of the spatial structure for a fixed time t for the time dependencies described in Fig. 15. The notation and the drawing style is the same as for Fig. 14. The times t of the snapshots are (a) $t=3000$, (b) $t=1000$, and (c) $t=1000$. We note that (a) and (b) show that the bursts continue indefinitely and that the arising spatial structures are small scale. The same applies to the noise-induced switching shown in (c). The time on the ordinates is in seconds and the abscissa is in scaled length units.

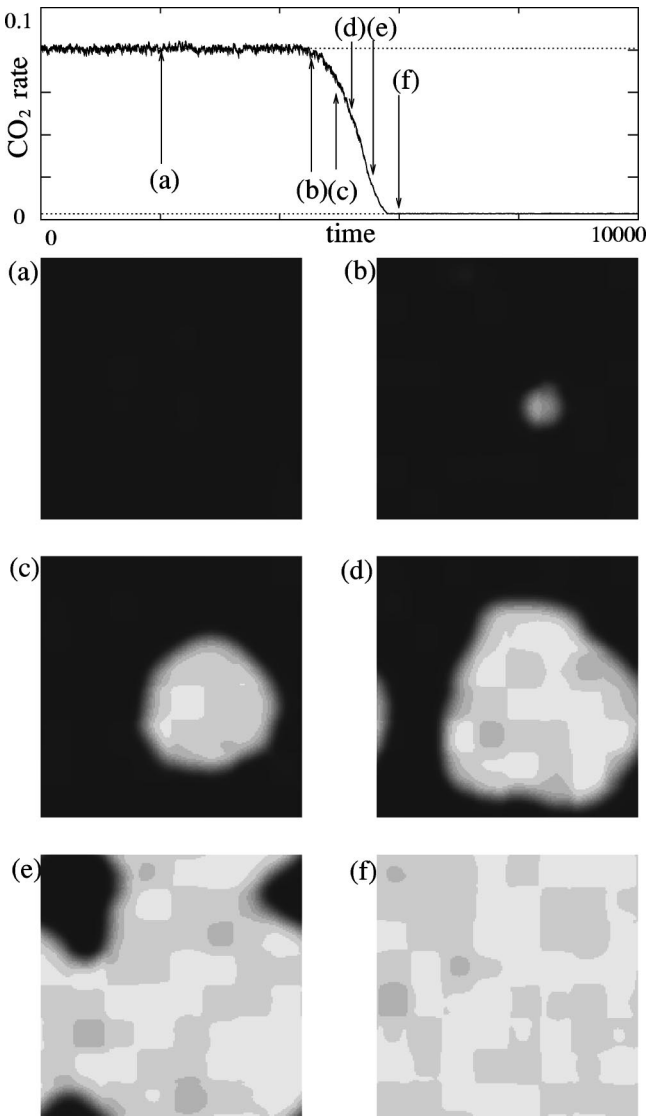

FIG. 17. Example of a long transient for the transition form the upper to lower branch as it arises in 2D simulations; $Y=0.12$ and $\Delta Y=0.025$. The box size is $L\times L=2\times 2$, Δx for the noise averaging is $\Delta x=0.25$, and the averaging time for the noise is $\tau_{noise}=9$ s. For the snapshots shown in Figs. 17 and 18 the minimal size of the squares visible in the plots corresponds to the area over which the noise is averaged. High values of CO correspond to white and low values to black. The times t for which the spatial snapshots are shown are marked in the time dependence of the CO_2 rate: (a) $t=2000$, (b) $t=4500$, (c) $t=5000$, (d) $t=5300$, (e) $t=5600$, and (f) $t=6000$. This sequence of snapshots clearly shows that nucleation takes place. In the top diagram the CO_2 rate is in arbitrary units and the time on the abscissa is in seconds.

effect of noise is predominantly a broadening of the probability distribution—as is expected—and an asymmetry as well as a small shift of the location of the maximum for parameter values on the lower branch close to the hysteresis loop. Inside the deterministically bistable regime the probability density (Figs. 5–8) broadens and the location of its maximum shifts away from the deterministic value of the starting location. In addition, there is, for moderate to high noise strength, the occurrence of an increasing asymmetry in the distribution, which is more pronounced when starting on the lower branch. These results compare well with those obtained from the numerical analysis: starting on the upper branch the probability density broadens first with increasing noise strength before it also starts to shift discernibly, while for a starting value on the lower branch, this shift away from the deterministic location of the starting value occurs even for small noise strength.

Near the boundary of the bistable regime the transitions from the smaller basin of attraction to the larger one proceed for small noise strengths via long transients (Fig. 13), while for larger noise strengths the time scales involved are shorter by about two orders of magnitude. The reason for this difference in time scales becomes clear, when space-time plots and snapshots of the spatial structures are analyzed (Fig. 14). In one case the transition is triggered by isolated nucleation sites far apart and proceeds via domain wall motion of a

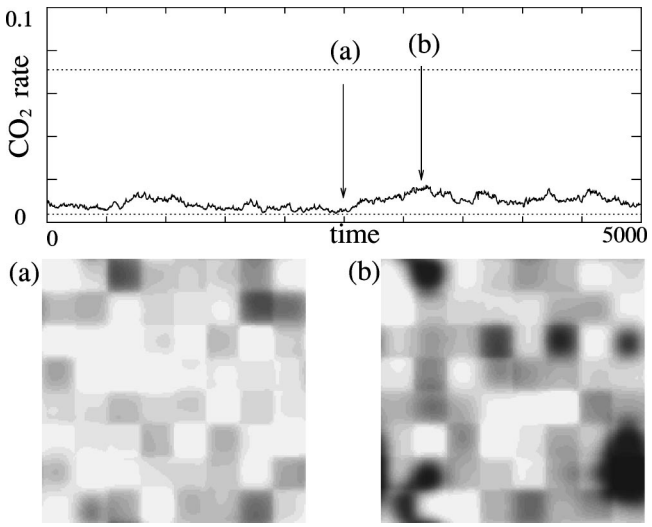

FIG. 18. For high noise strength there is a large region in parameter space for which one observes the upper or the lower branch with superposed bursts. Here we show the time dependence for bursts superposed on the lower noisy branch using the same color coding as for Fig. 17; $Y=0.11$ and $\Delta Y=0.09$. Snapshots of the spatial structure for a fixed time t for the time dependence shown on top are for (a) $t=2500$ and (b) $t=3200$. The bursting process occurs indefinitely. In the top diagram the CO_2 rate is in arbitrary units and the time on the abscissa is in seconds.

small number of walls while for the other case there is a high density of nucleation sites and the system fills in rather fast. The slow nucleation process is also clearly brought out in the 2D results shown in Fig. 17.

Increasing the noise strength further one observes in the experiments as well as in the simulations first bursts and then noise-induced switching (Fig. 15). In the 1D and 2D simulations this is brought out dramatically when space-time plots and spatial snapshots are analyzed (Figs. 16 and 18).

The experimentally and numerically observed behavior as a function of Y and the noise strength ΔY is summarized for the transient behavior and the asymptotic regime in Figs. 11 and 12, respectively.

Coming back to our Fig. 2 showing the n_{CO}-n_O diagram of the spatially homogeneous system in the deterministically bistable regime, we can conclude, both from our experimental and numerical results, that an increase of the applied noise strength leads to an increased band of n_{CO} and n_O values on both sides of the separatrix the system can have access to. In addition, the stable fixed points expand to an ''area.'' For large enough noise strength a noise-induced switching behavior can occur, since the system has noisy ''access'' to the whole parameter space.

As for the occurrence of spatially homogeneous behavior versus pattern formation on the surface our analysis shows that for sufficiently small noise spatially homogeneous noisy behavior prevails. With increasing noise strength we observe, depending on Y and ΔY, large scale spatial patterns (island formation), which nucleate and then coarsen via slow domain wall motion, or small scale spatial patterns with a short lifetime (reminiscent of spatiotemporal intermittency).

We would like to stress that, although we have made no adjustments with respect to the location and width of the hysteresis loop for experiments versus modeling, the phase diagrams Y versus ΔY for the transient as well as for the asymptotic (in time) behavior are very similar qualitatively and that there is almost quantitative agreement concerning the location and areas of most types of behavior. We conclude from this observation that the phase diagrams are rather insensitive to changes of the values of the diffusion coefficients by a factor of 2 or 3. Substantial changes in the phase diagrams are to be expected, however, when the diffusion coefficients are changed by orders of magnitude.

VI. CONCLUSIONS AND PERSPECTIVE

In the present paper we have shown that for the oxidation of CO on Ir(111) there is semiquantitative and even quantitative agreement between the effects of external noise imposed on the flux rate as observed experimentally and the results found from the modeling using reaction-diffusion equations suitably modified by additive and multiplicative noise. This close agreement can be traced back to the fact that all parameters occurring in the rate equations are known exceptionally well experimentally; a situation unknown for autocatalytic chemical reactions in bulk samples such as the Belousov-Zhabotinsky reaction.

In particular we note that in the region of parameters where one has a stationary hysteresis loop deterministically, we find both experimentally and theoretically, phenomena such as slow wall motion for the transition between the upper and lower branch, noise-induced bursts on both branches as well as noise-induced switching between the two branches for sufficiently large noise strength.

While the spatial patterns could not be observed experimentally, we could deduce the spatial patterns from the modeling in one and two spatial dimensions. It is most noteworthy that the long transients observed experimentally first deterministically [24] and here in the presence of noise can be naturally associated with wall motion.

It will be most interesting to investigate similar reactions on other well-characterized surfaces. This would allow a further enhancement of our understanding of systems that include both spatial degrees of freedom and various noise sources, a field which is basically wide open, since typically there are only models without any concrete experiments to compare with.

ACKNOWLEDGMENTS

Y.H. thanks the Alexander von Humboldt Foundation for financial support. H.R.B. thanks the Deutsche Forschungsgemeinschaft for partial support of his work.

[1] N. van Kampen, *Stochastic Processes in Physics and Chemistry* (North-Holland, Amsterdam, 1983).
[2] H.A. Kramers, Physica (Amsterdam) **7**, 284 (1940).
[3] R. Graham and H. Haken, Z. Phys. **243**, 289 (1971); **245**, 141 (1971).
[4] H. Risken, Z. Phys. **251**, 231 (1972).
[5] H. Risken, *The Fokker-Planck Equation* (Springer, Berlin, 1989).
[6] A. Schenzle and H. Brand, Opt. Commun. **27**, 485 (1978).
[7] A. Schenzle and H. Brand, Opt. Commun. **31**, 401 (1979).
[8] M. Bär, Ch. Zülicke, M. Eiswirth, and G. Ertl, J. Chem. Phys. **96**, 8595 (1992).
[9] A. Mikhailov and G. Ertl, Science **272**, 1596 (1996).
[10] M. Tammaro, M. Sabella, and J.W. Evans, J. Chem. Phys. **103**, 10 277 (1995).
[11] D.-J. Liu and J.W. Evans, J. Chem. Phys. **117**, 7319 (2002).
[12] J.W. Evans, D.-J. Liu, and M. Tammaro, Chaos **12**, 131 (2002).
[13] A. Schenzle and H. Brand, Phys. Rev. A **20**, 1628 (1979).
[14] W. Horsthemke and R. Lefever, *Noise Induced Transitions* (Springer, Berlin, 1984).
[15] S. Kabashima, S. Kogure, T. Kawakubo, and T. Okada, J. Appl. Phys. **50**, 6296 (1979).
[16] H.R. Brand, S. Kai, and S. Wakabayashi, Phys. Rev. Lett. **54**, 555 (1985).
[17] R. Imbihl and G. Ertl, Chem. Rev. (Washington, D.C.) **95**, 697 (1995).
[18] G. Ertl, Science **254**, 1750 (1991).
[19] H.H. Rotermund, W. Engel, M. Kordesch, and G. Ertl, Nature (London) **343**, 355 (1990).
[20] M. Berdau, A. Karpowicz, G.G. Yelenin, K. Christmann, and J.H. Block, J. Chem. Phys. **106**, 4291 (1997).
[21] M. Ehsasi, M. Berdau, T. Rebitzki, K.-P. Charlé, K. Christmann, and J.H. Block, J. Chem. Phys. **98**, 9177 (1993).
[22] Yu. Suchorski, J. Beben, E.W. James, J.W. Evans, and R. Imbihl, Phys. Rev. Lett. **82**, 1907 (1993).
[23] C.A. Wolf and B.E. Nieuwenhuys, Catal. Today **70**, 287 (2001), and references therein.
[24] S. Wehner, F. Baumann, and J. Küppers, Chem. Phys. Lett. **370**, 126 (2003).
[25] S. Wehner, F. Baumann, M. Ruckdeschel, and J. Küppers, J. Chem. Phys. **119**, 6823 (2003).
[26] E.G. Seebauer and C.E. Allen, Prog. Surf. Sci. **49**, 265 (1995).